An Observational, Spatially Explicit, Stability-Based Estimate of the Wind Resource off the Shore of North Carolina

N. THOMAS

Department of Atmospheric and Oceanic Science, University of Maryland, College Park, College Park, Maryland

H. SEIM AND S. HAINES

Department of Marine Sciences, University of North Carolina at Chapel Hill, Chapel Hill, North Carolina

(Manuscript received 23 March 2015, in final form 11 August 2015)

ABSTRACT

As part of ongoing studies of the feasibility of utility-scale wind energy off the shore of North Carolina, winds at 80-m elevation are estimated with a stability-based height-adjustment scheme. Data sources are level-3 daily Advanced Scatterometer (ASCAT) 10-m wind fields as measured by the *MetOp-A* satellite, North American Regional Reanalysis (NARR) estimates of near-surface atmospheric temperature and humidity, and the National Climatic Data Center's optimally interpolated Advanced Very High Resolution Radiometer (AVHRR-OI) sea surface temperature (SST). A height-adjustment assuming neutral atmospheric stability provides reference conditions. The SST from AVHRR-OI was more accurate than SST from NARR and was used with NARR atmospheric data to represent atmospheric stability in the study region. The 5-yr average of the ASCAT 10-m winds is 6.5–9.0 m s^{-1} off the shore of North Carolina, with the strongest winds found over the Gulf Stream. Neutral-scheme 80-m wind speeds are 7.5–10.5 m s^{-1} and follow the same spatial pattern. The stability-based scheme produces an 80-m wind field with significantly different spatial wind patterns, with greater wind speeds than the neutral scheme in coastal regions where stable atmosphere conditions occur and lesser wind speeds than the neutral scheme farther offshore where unstable conditions are prevalent. The largest differences between the schemes occur in winter and spring when and where stable atmospheric conditions are most common. Estimated power inshore from the 100-m isobath with the neutral scheme yields average values of 400–800 W m^{-2}, whereas the stability-based-scheme values are 600–800 W m^{-2}. Capacity factors vary between 30% and 55%, with values in excess of 40% common in coastal areas off North Carolina.

1. Introduction

Offshore wind resource assessments over the continental shelf off North Carolina (e.g., Musial and Ram 2010) have suggested that tens of gigawatts of power generation potential exist for offshore wind farms. An initial assessment undertaken by the University of North Carolina at Chapel Hill (UNC) took advantage of a variety of in situ historical observations and employed simple height-adjustment schemes (a power-law and log-layer formulation) to estimate turbine-height winds and power potential (UNC 2009; Seim et al. 2010). Subsequent work (Seim et al. 2012) has investigated a variety of more sophisticated height-adjustment schemes and established that level-3 (L3) daily 10-m satellite Advanced Scatterometer (DASCAT) winds (Bentamy and Croize-Fillon 2012) estimated by the Advanced Scatterometer (ASCAT) program (2008–present) are consistent with buoy-based winds over the area of interest. Here we describe implementation and evaluation of a stability-based height-adjustment scheme applied to the DASCAT winds to provide a spatially explicit estimate of the wind resource at typical turbine hub height for the entire exclusive economic zone off the shore of North Carolina.

Motivation for this reexamination comes from recognition of the influence that oceanic conditions off the shore of North Carolina have on the lower atmosphere there and the ongoing lease process by the U.S. federal government. Large spatial changes in average sea

Corresponding author address: H. Seim, Marine Sciences, CB#3300, 3202 Venable Hall, University of North Carolina at Chapel Hill, Chapel Hill, NC 27599.
E-mail: hseim@email.unc.edu

DOI: 10.1175/JAMC-D-15-0090.1

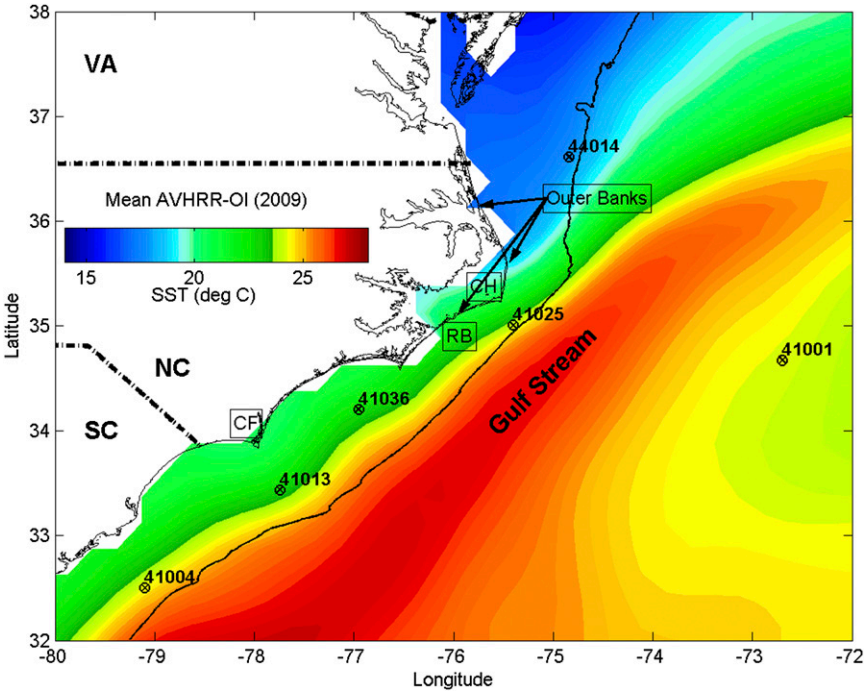

FIG. 1. Map of study area showing the position of the buoys used in the study and the location names [Raleigh Bay (RB), Cape Hatteras (CH), and Cape Fear (CF)] used in the text overlaid on the mean sea surface temperature for 2009 from the AVHRR-OI product. The 100-m depth contour is shown as a black line off the shore of the coastline.

surface temperature (SST) off the shore of North Carolina are typically produced by the warm, poleward flow of the Gulf Stream and cool, equatorward flow over the mid-Atlantic continental shelf that produce strong variations in static stability of the overlying lower atmosphere. We seek here to clarify the dependence of turbine-height winds (30–150 m above sea level) off North Carolina on atmospheric stability. We document the sign and strength of the change in wind speed relative to neutral atmospheric conditions, as well as its variation alongshore and across shore and over time. The Bureau of Ocean Energy Management (BOEM) has, since 2011, been moving forward with the identification of wind energy areas off the shore of North Carolina, providing further motivation for this study. We examine areas over the continental shelf of possible development (regions 1–3 below) as a way to dovetail with BOEM activities.

Similar efforts to study regional wind patterns as they relate to the wind energy resource have been conducted off Delaware (Sheridan et al. 2012); in the North Sea (Karagali et al. 2014), Mediterranean Sea (Furevik et al. 2011), Ionian Sea (Karamanis et al. 2011), Yellow Sea (Lee et al. 2013), and China Sea (Zheng et al. 2013); and off southeast Brazil (Pimenta et al. 2008), to name a few recent studies. Many of these studies have employed satellite-based wind observations as a component of the observational database. Most have used QuikSCAT winds because of their availability from the late 1990s until 2009. In the majority of the studies above the comparison of in situ and satellite winds have indicated only a small bias in speed and direction.

This study area includes the Gulf Stream, which during most times of the year exhibits a strong ocean thermal front that has been documented to influence the low-level (10 m) mesoscale wind field (O'Neill et al. 2012), leading to increased low-level winds where SST is elevated. A notable feature of the region is a persistent area of cooler water over the continental shelf and slope just inshore from the Gulf Stream (Fig. 1), where stable atmospheric conditions are common during part of the year. The juxtaposition of these two areas clearly influences the 10-m wind field and can be expected to impact hub-height winds as well. These conditions present a challenge for implementing a stability-based height adjustment that can capture correctly the strong horizontal variations that characterize the area off the shore of North Carolina.

We first present the methods used to adjust satellite winds to turbine hub height. The data description section evaluates remotely sensed and model data against buoy observations in order to identify the least biased dataset to use in the stability-based height adjustment.

The results section presents the gridded results of the mean wind fields, the seasonal cycle, interannual variability, and the mean and varying estimated power. The discussion focuses on the limitations of the approach.

2. Methods

a. Height adjustment

Monin–Obukhov similarity (MOS) scaling, with some modifications to improve its application over the oceans (including variations in surface roughness with wind speed), has been found to adequately represent the variations in surface fluxes and wind shear in a number of settings and is a simple way to account for variations in atmospheric stability at low elevations over the ocean. Implementations of MOS scaling have found wide application and continue to be refined (Fairall et al. 1996; Fairall et al. 2003; Edson et al. 2013). In these implementations, stability is determined by the magnitude and sign of the buoyancy flux between the ocean and atmosphere. The buoyancy flux is related to the sum of the heat and moisture fluxes. Unstable conditions, which exist when the flux of buoyancy is out of the ocean and by convention is negative, are associated with convection, enhanced near-surfaces fluxes, and reduced near-surface wind shear, whereas stable conditions, which are favored when the buoyancy flux is positive, are associated with reduced near-surface fluxes and increased near-surface wind shear (see, e.g., Garratt 1992). Use of these formulations requires a number of variables in addition to wind speed to be measured simultaneously, specifically, surface air temperature (SAT), relative humidity, and SST. A commonly available implementation of the Coupled Ocean–Atmospheric Response Experiment bulk algorithm, version 3.0 (COARE v3.0, Fairall et al. 2003), was used. The wind speed is adjusted using

$$u(z_{\text{new}}) = u_r + \left(\frac{u_*}{k}\right)\left[\ln\left(\frac{z_{\text{new}}}{z_r}\right) - \Psi\left(\frac{z_{\text{new}}}{L}\right) + \Psi\left(\frac{z_r}{L}\right)\right],$$

where $u(z_{\text{new}})$ represents estimated wind speed at turbine height z_{new}, u_r is the wind speed at the reference height z_r (10 m for the DASCAT winds), k is von Kármán's constant, u_* is the friction velocity, Ψ is an empirically determined function, L is the Obukhov length:

$$L = \frac{u_*^2}{kB_0}, \quad \text{and}$$

$$B_0 = \left(\frac{g}{T_v}\right)[T^*(1 + 0.61Q) + 0.61TQ^*]$$

is the buoyancy scale, such that the buoyancy flux is $-(u_*B_0)$. Here g is the acceleration due to gravity, T_v is virtual temperature, Q is specific humidity, and T^* and Q^* are scaling parameters related to the air–sea temperature difference (SAT − SST) and the departure of the humidity from saturation near the ocean surface (Fairall et al. 1996; Godfrey and Beljaars 1991). Use of this stability-based height adjustment, referred to below as the "stability-based scheme," requires appropriate sources of ancillary data on the same time and space scales as the ASCAT winds. Limitations to the approach are presented in the discussion.

A form of height adjustment that assumes neutral atmospheric stability is used for comparison. This scheme is simple to implement because it requires only wind observations at a specified height above the sea surface:

$$u(z_{\text{new}}) = u_r + \left(\frac{u_*}{k}\right)\ln\left(\frac{z_{\text{new}}}{z_r}\right).$$

The friction velocity is a function of the drag coefficient C_{d10n} and the wind speed at 10-m height

$$u_* = \sqrt{C_{\text{d10n}}}u_{10}.$$

A limitation in our use of these formulations is that the wave field is represented by the wind speed alone, which introduces uncertainty in the application of these simple schemes from a lack of dependence on wave age, especially in shallow waters and in fetch-limited settings (Fairall et al. 1996). While recent formulations allow for inclusion of wave field observations (Fairall et al. 2003), we did not pursue that as part of this study.

We identify sources of gridded values for the ancillary fields in the following section. To validate these datasets the variables are compared to buoy-based observations. Prolonged instances of missing dewpoint data for several buoy stations led to the need for a substitution. A linear fit was produced between the air temperature and dewpoint values (when both were available). This was used to produce values of dewpoint at times when air temperature was available. The substituted dewpoint was found to produce no significant difference in the estimation of the buoyancy flux and significantly increased the time frame for possible analysis.

b. Power and capacity factor

Power available from the wind is given as the power density (power per unit area) P:

$$P = \frac{1}{2}\rho u^3,$$

where $\rho = 1.2\,\text{kg}\,\text{m}^{-3}$ is the density of air near the sea surface, assumed to be a constant. This theoretical calculation is useful for comparison with other areas but

TABLE 1. Mean difference between the buoy, NARR, and DASCAT winds ($m\,s^{-1}$) over 2008–12. Buoy winds are measured at 5 m, so here they are extrapolated to 10 m using both the neutral and stability-based schemes. NARR and DASCAT winds were subtracted from buoy winds to obtain the mean difference; 95% confidence intervals are shown where the difference is statistically different than zero.

Station	Mean buoy wind speed (neutral scheme)	Mean difference (stability scheme) buoy − NARR	Mean difference (neutral scheme) buoy − NARR	Mean difference (stability scheme) buoy − DASCAT	Mean difference (neutral scheme) buoy − DASCAT
41001	7.80	0.14 ± 0.06	0.09 ± 0.06	−0.18 ± 0.13	0
41004	6.95	1.42 ± 0.04	1.44 ± 0.03	0.08 ± 0.06	0.33 ± 0.06
41013	7.12	1.66 ± 0.04	1.72 ± 0.03	0	0.26 ± 0.06
41025	7.75	0.78 ± 0.06	0.86 ± 0.04	0	0.14 ± 0.09
44014	6.88	0.34 ± 0.05	0.29 ± 0.04	0	0
41036	7.28	1.76 ± 0.04	1.79 ± 0.04	0	0.16 ± 0.08

does not represent the actual realizable power available because of the practical constraints of extracting energy with a turbine. A power curve can be used (e.g., Pimenta et al. 2008) to estimate actual power that can be generated; it directly relates wind speed to power output by a turbine. Most power curves for large offshore turbines used in utility-scale wind farms are similar in shape, with cut-in speeds of 2–3 $m\,s^{-1}$, reaching rated power around 10–12 $m\,s^{-1}$, and with a cut-out speed of 25–30 $m\,s^{-1}$. The power generated depends on the maximum output of the turbine and the wind field in which the turbine is placed, and it can be generalized by reporting the capacity factor, or the average power output divided by the maximum power output. We here use an approximate power curve for a Vestas V90, an older 3-MW turbine, to permit comparison with the earlier study of capacity factor off North Carolina (Seim et al. 2010). See Lee et al. (2013) for a comparison of power curves for a variety of turbines.

3. Data description

Below we describe the methods for identifying data products used in the analysis, organized by subsections for specific variables. A variety of sources were used. The L3 DASCAT product from the French Research Institute for Exploitation of the Sea (Bentamy and Croize-Fillon 2012; CERSAT 2012) provides temporally and spatially gridded, daily estimates of wind speed on a 25-km spatial grid starting in January 2008. This C-band scatterometer is calibrated to produce 10-m neutral winds (Hersbach 2010) relative to the ocean surface. After exploring possible sources for SST, SAT, relative humidity, and barometric pressure we found that the North American Regional Reanalysis (NARR) product from the National Centers for Environmental Prediction (Mesinger et al. 2006; PSD 2006) was available for the time period of interest and largely compatible in spatial resolution (roughly 32 km) with the DASCAT winds. In situ observations in the study area are available from six National Data Buoy Center (NDBC) buoys off the shore of North Carolina over the time period 2008–12. Figure 1 shows the locations of the buoys and place names used to describe the results. Accuracies of individual buoy observations are presented online (http://www.ndbc.noaa.gov/rsa.shtml); for the long time averages formed as part of this study, the standard error, given as the standard deviation divided by the square root of the number of independent data points, is used to establish uncertainty.

a. Winds

We first examine the NARR wind field through a comparison with the buoy-based winds, pairing the 3-hourly estimates from NARR output with hourly buoy winds interpolated to the times of the NARR winds and extrapolated to 10-m height. We found the mean NARR wind speeds to be biased low relative to buoy-based wind observations by as much as 1.79 $m\,s^{-1}$ (Table 1). The differences were dependent on which height-adjustment scheme was used as well as the location, with offshore regions producing the smallest differences and areas close to the coast exhibiting the greatest differences. The exception to this is station 44014, where persistently stable conditions lead to reduced 5-m winds measured by the buoys relative to locations with neutral or unstable conditions. NARR systematically underestimates wind speed as compared with the buoys.

We next compare the DASCAT wind field against the buoy winds. The 10-m neutral wind was formed as

$$u_{10n} = u(z) + \left(\frac{u_*}{k}\right)\left[\ln\left(\frac{10}{z}\right) + \psi\left(\frac{z}{L}\right)\right],$$

using the buoy observations and the COARE v3.0 algorithms. We also form the stability-dependent 10-m wind. The DASCAT L3 daily product uses objective mapping to define a daily wind speed and independently a daily wind vector (expressed as vector components; Bentamy and Croize-Fillon 2012). The reported daily wind speed for the study area is typically greater than the

magnitude of the daily wind vector, presumably because the objective mapping averages multiple overpasses in a given day for latitudes poleward of about 30°. The appendix evaluates the correlation between the DASCAT winds and buoy observations to identify how best to interpret the DASCAT product. The DASCAT winds are more consistent with the stability-dependent 10-m wind (Table 1), except at the one buoy located in deep water (41001). Though this result is somewhat surprising, Portabella and Stoffelen (2009) found ASCAT winds to be consistent with both neutral and actual winds. The DASCAT winds are therefore treated in this study as actual winds in the height-adjustment process because of this finding and because it minimizes adjustments to the observed winds.

b. SST and SAT

SST and 2-m SAT and dewpoint were found to be overestimated by NARR when compared with the buoys. The mean difference between NARR and buoy-measured SST for 2008–12 ranged from 1.2° to 3.0°C, with the largest difference being near shore and north of Cape Hatteras. Furthermore, the SST differences are much greater in the winter than in the summer (Fig. 2). The mean SAT difference between NARR and the buoys for 2008–12 was in the range of 0.9°–1.9°C, and the largest difference was again near shore and north of Cape Hatteras. A seasonal cycle similar to the SST difference exists in the SAT difference, where the values are greater in the winter than in the summer, indicating that NARR is misrepresenting the wintertime low temperatures (Fig. 2). The mean difference between NARR and buoy-measured dewpoint for 2008–12 ranged from 2.2° to 3.7°C. Differences for these three parameters are summarized for four different regions (defined in the next paragraph) in Table 2. In addition to these, barometric pressure was examined and it compared well for NARR and the buoy measurements. Values were not significantly different over the 2008–12 time period.

Of relevance for the MOS extrapolation scheme is the value of B_0, largely set by the sea–air temperature difference (SST − SAT). Unstable atmospheric conditions are likely to occur when SST − SAT is positive, and stable conditions are likely to occur when it is negative. A comparison of SST − SAT reveals that NARR data alone overestimate this temperature difference such that unstable conditions persist over the entire area of interest. The buoy-based differences indicate consistent spatial structure to stability of the near-surface atmosphere. Stable conditions occur on the shelf north of Cape Hatteras (designated region 1, near station 44014) and in the nearshore waters south of Cape Hatteras (designated region 3, near station 41013) during winter and early spring. Importantly, notice for both stations in Fig. 2 that the NARR data frequently do not achieve negative (stable) values of SST − SAT when the buoys do.

To better capture the dynamics of the regions that exhibit persistently stable conditions, a substitute SST product was sought. A number of daily products are now available that utilize optimal interpolation (OI) and a blend of infrared and microwave radiometers and in situ observations. All are global products but at varying spatial resolution. The 25-km-resolution National Climatic Data Center optimally interpolated Advanced Very High Resolution Radiometer (AVHRR-OI; Reynolds et al. 2007; NCDC 2007) was found to best represent SST along the North Carolina coast relative to buoy-based observations, though a bias is still present (Table 2). Other products, though available at finer spatial resolution, often fail to accurately capture the cooler nearshore waters in winter and north of Cape Hatteras.

When the AVHRR-OI SST product is used in combination with the NARR SAT, the SST − SAT difference exhibits periods of stable conditions in the same locations as the buoy observations but is biased toward greater stability and weaker unstable conditions. Figure 3 shows B_0 estimated by the buoys, NARR, and the combination of SAT data from NARR and SST from AVHRR-OI. This shows that NARR data alone estimate a more negative B_0, particularly in the winter. We find that the NARR and AVHRR-OI data combination leads to an estimate of B_0 that is more comparable with the buoy data. In fact, B_0 is slightly overestimated at certain times. This indicates that the bias has shifted to the other direction, and the frequency and intensity of stable conditions are now being somewhat overestimated.

The exception to this pattern is station 41025 (Fig. 3b). This is a unique part of the study region because of its proximity to the Gulf Stream. Both NARR and the satellite combination are unable to capture the temperatures completely accurately because of the abruptness and proximity of the landward edge of the Gulf Stream, which produces rapid changes in temperature at this location (Fig. 1).

4. Results

The COARE v3.0 stability-based height adjustment has been implemented to estimate winds at 80 m above sea level, making use of the DASCAT 10-m winds, treated as actual winds, the AVHRR-OI SST and the NARR SAT, relative humidity, and air pressure. The neutral stability height adjustment is formed as a reference. The smallest temporal resolution possible is daily, set by the availability of the chosen satellite products.

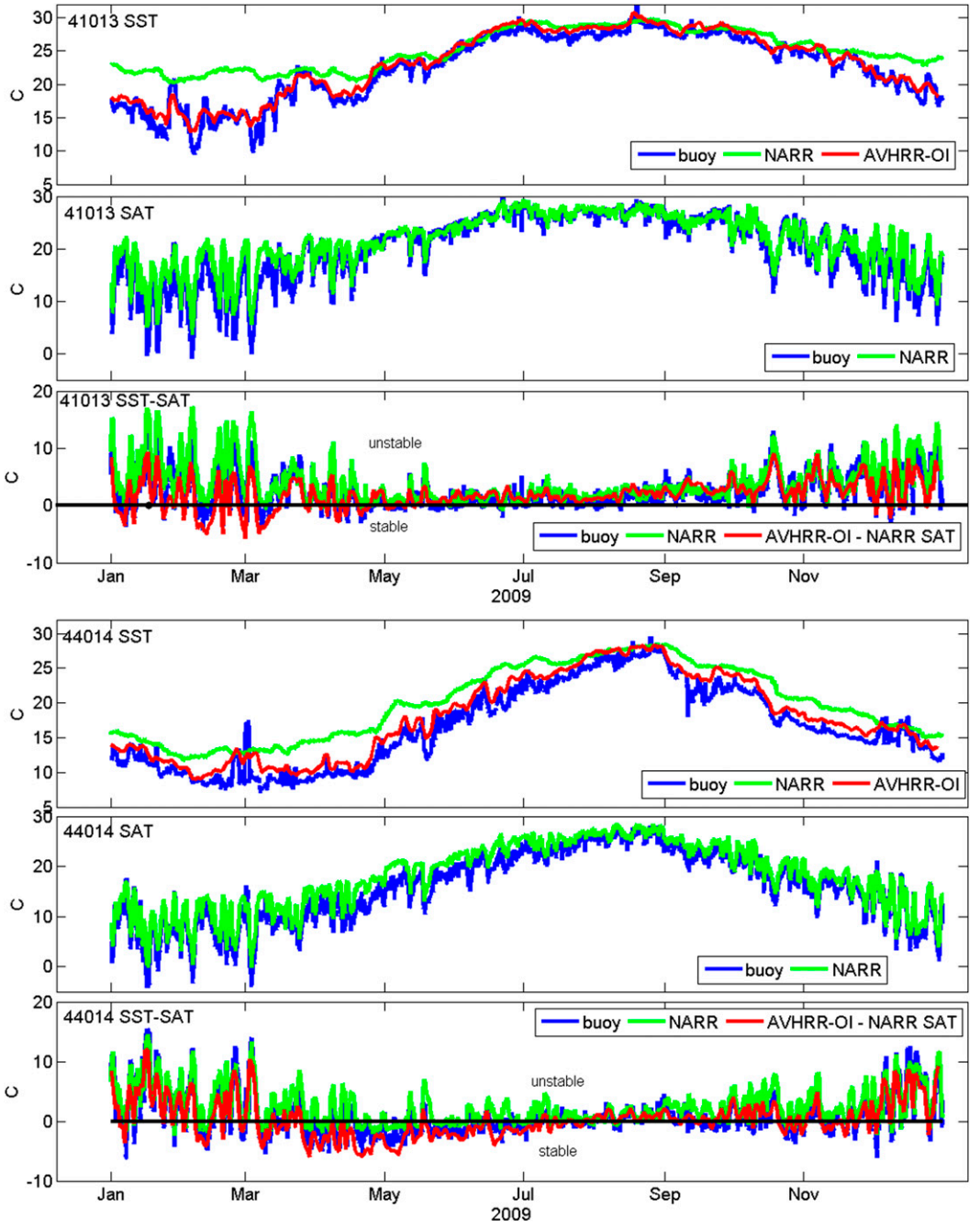

FIG. 2. SST, SAT, and SST − SAT as estimated by NARR (green), measured by the buoys (blue), and the AVHRR-OI SST product (red) for station (top) 41013 (off the shore of Cape Fear) and (bottom) 44014 (off the shore of Virginia) for 2009. Positive (negative) values for SST − SAT are indicative of unstable (stable) lower-atmospheric conditions.

The 80-m wind estimates were compared against buoy winds adjusted to 80 m using the neutral and stability-based schemes in order to validate the final result (Table 3). The neutral-scheme estimate of the 80-m winds is not significantly different from zero at three of the buoys and is underestimated by the DASCAT-based wind when compared to the buoys at three of the locations. For the estimate using the stability-based scheme, the difference is significant at three locations, with the DASCAT-based wind overestimating the winds at 41013 near Cape Fear, 44014 off the northern Outer Banks and 41036. The reasons for these discrepancies

TABLE 2. Mean difference between AVHRR-OI and buoy SST and NARR and buoy SST, SAT, and dewpoint (DP) for 2008–12. Buoy values were subtracted from AVHRR-OI and NARR values.

Region	Station	Mean SST difference (°C) AVHRR-OI − buoy	Mean SST difference (°C) NARR − buoy	Mean SAT difference (°C) NARR − buoy	Mean DP difference (°C) NARR − buoy
Sargasso Sea	41001	0.98 ± 0.03	1.22 ± 0.02	0.86 ± 0.04	3.6 ± 0.06
1	41013	0.93 ± 0.04	2.58 ± 0.04	1.58 ± 0.03	3.21 ± 0.04
2	41025	2.18 ± 0.13	1.20 ± 0.07	1.30 ± 0.04	2.67 ± 0.06
3	44014	1.3 ± 0.04	3.01 ± 0.03	1.92 ± 0.02	2.19 ± 0.09

are explored below. We note that 80-m winds formed using the stability-based scheme but assuming the DASCAT wind are 10-m equivalent neutral winds exhibit mean differences from 80-m buoy winds that are somewhat greater than those in Table 3 (not shown).

a. 80-m wind speed

Daily values of estimated 80-m wind speed were produced using neutral and stability-based schemes for 2008–12. These daily estimates reveal significant departures from neutral stability when using the stability-based scheme. These departures vary with geographic location, as shown in Fig. 4, which displays the average conditions over 2008–12. (In this figure, and for most subsequent results, we choose to contour the results in maps, which makes it easier to identify the range of values plotted, though the contouring algorithm occasionally produces confused results near the coast because of the irregular boundary.) Figure 4b illustrates how strongly unstable conditions (SST − SAT > 2°C) dominate over the Gulf Stream and in the Sargasso Sea on average. In these regions the stability-based winds at 80 m are typically 0.5 m s^{-1} less than expected if neutral conditions are assumed. Stable conditions are most common in the region north of Cape Hatteras. In this region, the average SST − SAT is less than 0 and the stability-based winds at 80 m are significantly greater than expected if neutral stability is assumed. This is because of the increased vertical shear associated with stable conditions, and the result is a speed difference of up to 2 m s^{-1} in the average.

It is worth noting that the spatial maximum in wind speed associated with the Gulf Stream seen in the average 10-m winds (Fig. 4a) is less apparent in the stability-based 80-m wind estimate (Fig. 4d). The latter wind field exhibits less zonal variation seaward of the 100-m isobath, as might be expected at higher elevations in the atmosphere where the surface boundary influence is diminished. The meridional increase in wind speed is consistent with stronger midlatitude winds.

To better understand the spatial variations in the departures between the two height-adjustment schemes, the seasonal cycle, formed with the data over the 5-yr time period, is explored. Figure 5 shows the seasonal progression of estimated 80-m wind speeds from both schemes in three coastal regions of interest, formed with data from the entire 5-yr period of 2008–12. As a reference, 80-m height-adjusted winds from buoy observations in each region are also shown, as symbols. In general, winds are greatest in wintertime, with the peak time varying with location and height-adjustment scheme used, and least in the summer, reaching a minimum in August. In region 1, off the northern Outer Banks, stable conditions are often present from winter through late spring (January–June) because of the large temperature difference between the ocean surface and overlying air. This is the only region where, on average, SAT exceeds SST (Fig. 4b). Southward flow of cold waters in the Mid-Atlantic Bight helps maintain cool SSTs, in contrast to the SATs in the eastward flow of air that has been warmed over the continent. This time period is when the stability-based estimate shows the greatest departure from the 80-m wind estimate assuming neutral conditions, in the buoy-based and DASCAT-based estimates. The departure is larger and lasts longer in the DASCAT-based estimates. Region 2, off the central coast of North Carolina in Raleigh Bay (RB in Fig. 1), exhibits unstable conditions through most of the year, and as a result it displays a difference between schemes of about 0.5 m s^{-1}, with the neutral-based scheme estimating greater winds. In the spring (March–May), the neutrally stable conditions in this region lead to a similar prediction of the 80-m winds from both schemes. Finally, region 3, the southern end of the North Carolina coastal area, exhibits stable conditions in winter (January–April) in the DASCAT-based estimates, which lead to the largest difference between schemes in this season. The buoy-based estimates exhibit unstable conditions except during March and April when neutral or weakly stable conditions occur.

The comparison of the gridded estimates with the buoy estimates of stability-based 80-m winds in Fig. 5 suggests a bias of the gridded estimates toward greater wind speeds under stable atmospheric conditions. This finding is consistent with the bias of B_0 toward more

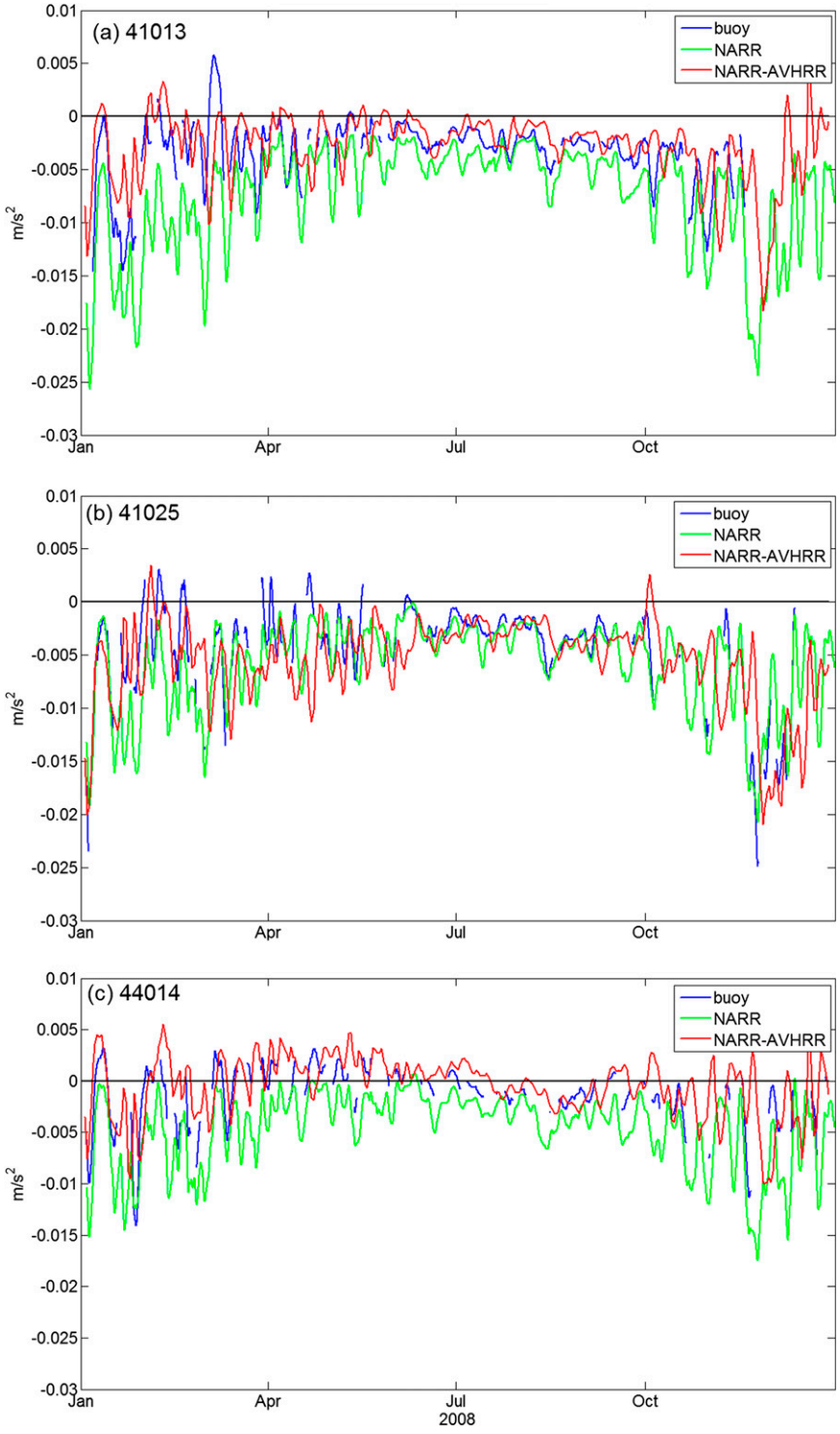

FIG. 3. B_0 comparison for stations (a) 41013, (b) 41025, and (c) 44014. Shown are estimates of B_0 using the three data combinations: all buoy data (blue), all NARR data (green), and NARR-AVHRR-OI (red).

TABLE 3. Mean difference with 95% confidence intervals between 80-m winds estimated with buoy data and 80-m winds estimated from the DASCAT/NARR/AVHRR combination of data over 2008–12. Zero values indicate no significant difference.

Station	Neutral-scheme mean difference	Stability-scheme mean difference (buoy − DASCAT/NARR/AVHRR)
41001	0	0
41004	0.47 ± 0.22	0
41013	0.33 ± 0.22	−0.29 ± 0.22
41025	0.32 ± 0.30	0
44014	0	−0.70 ± 0.30
41036	0	−0.53 ± 0.27

positive (stable) values when using the combination of SAT from NARR and SST from AVHRR-OI. At times when atmospheric stability is neutral or unstable, the gridded and buoy estimates are comparable.

Spatial structure of interannual variability over 2008–12 is assessed as the standard deviation of the annual averages (Fig. 6). It is computed for the neutral and stability-based extrapolation schemes. Over much of the study area the standard deviation is similar at 0.1–0.3 m s^{-1}. One maximum occurs on the eastern boundary of the domain between 33° and 36°N, likely associated with variation in where the Gulf Stream leaves the continental shelf, the location of which is known to vary with time and likely explains the higher deviation. Another maximum occurs on the shelf, reaching a maximum closest to the coastline. The main difference between the two depictions is the maximum in the stability-based standard deviations off the northern Outer Banks that is absent from the neutral-scheme standard deviations. The nearshore maxima are associated with differences in minimum air temperatures from year to year, with cooler years producing stronger wind speeds. The maximum off the northern Outer Banks in the stability-based standard deviations reflects variations in the spatial extent of stable atmospheric conditions from year to year. Importantly, the maximum standard deviations are about 0.5 m s^{-1} suggesting that interannual variability is typically 1 m s^{-1} or less.

b. *Power density and capacity factor*

To better understand and quantify the wind resource, the power is estimated. Figure 7 shows the average power estimates over 2008–12 formed using the 80-m wind estimates from both schemes. Not surprisingly, the power density estimates (Figs. 7a,b) have a very similar pattern to the 80-m wind speed estimates, given the cubic relationship between the two. The neutral-based estimate of power density rises from minima of 400 W m^{-2} at the coastline to a maximum of 1000 W m^{-2}

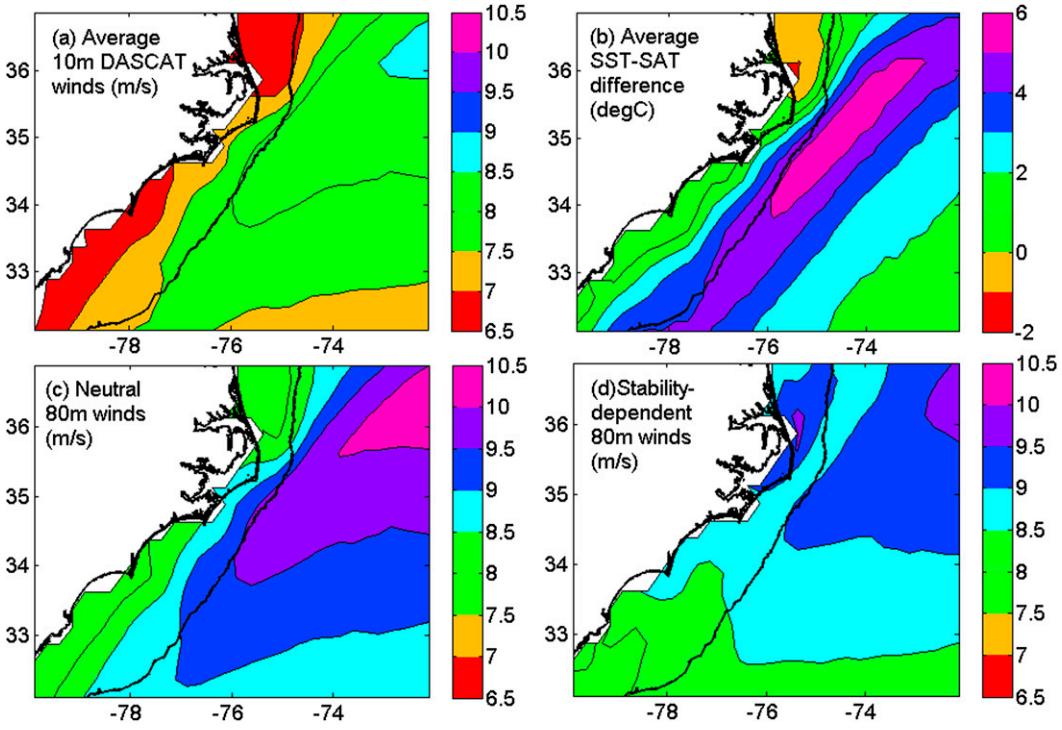

FIG. 4. Averages over the entire time range (2008–12) for (a) daily ASCAT 10-m winds, (b) AVHRR-OI SST-NARR SAT, (c) neutral-based estimate of the 80-m winds, and (d) stability-based estimate of the 80-m winds.

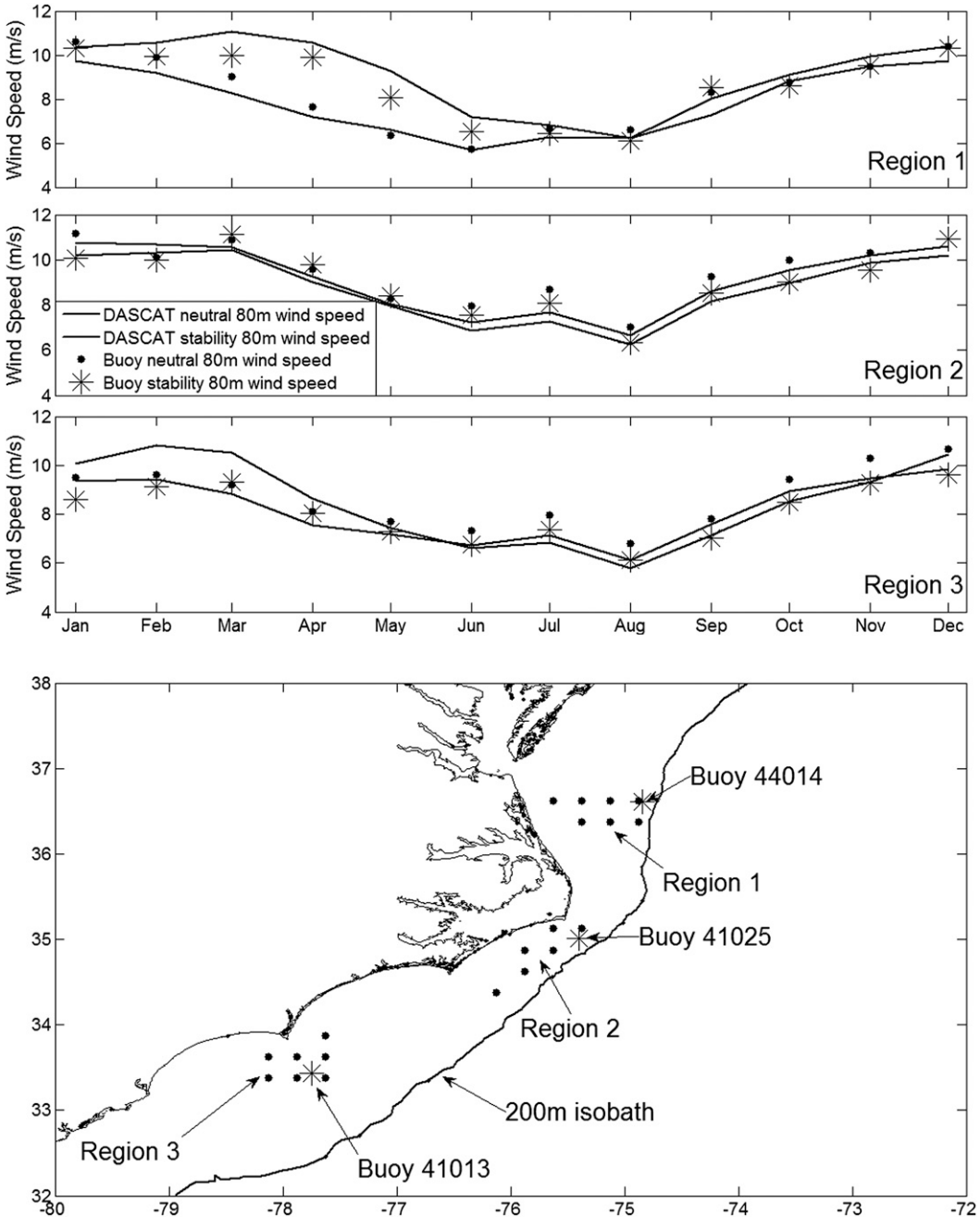

FIG. 5. Seasonal progression of the estimated wind speeds from both schemes. The locations of the DASCAT winds averaged to define each region are shown by dots in the map, and the buoy location is marked with a star.

over the Gulf Stream. The stability-based estimate is more uniform with values of 600–800 W m^{-2} off North Carolina, lower values to the south, and a weak maximum in the northeast portion of the study area. The power density estimates differ the most over the shelf off the northern Outer Banks, where stable conditions are common, with the stability-based estimate being greater by approximately 200 W m^{-2}.

Figures 7c and 7d depict the capacity factor, formed using a power curve for a Vestas V90 3-MW turbine [see Lee et al. (2013) for a comparison of this power curve with other large offshore turbines]. While the general patterns remain the same to those of the power density, there are some changes due to the inclusion of practical limitations in power generation such as cut-in and cut-out speeds. The neutral stability scheme predicts capacity

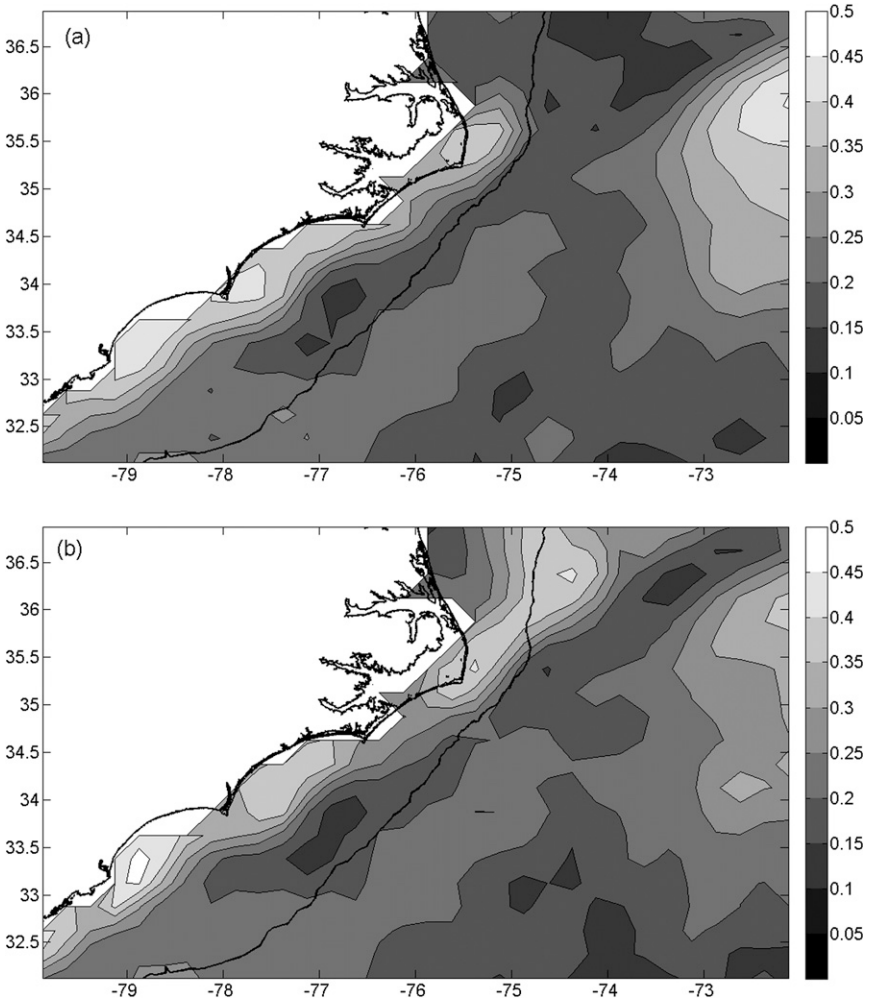

FIG. 6. Standard deviation ($m\,s^{-1}$) of estimated 80-m wind speed for the 5-yr time period for the (a) neutral scheme and (b) stability scheme.

factors of 40% or greater across the central shelf off North Carolina and on the outer shelf of southern North Carolina and maximum values over the Gulf Stream in excess of 50%. The stability-based scheme is similar on the central and south shelf but noticeably larger on the shelf off northern North Carolina.

Finally, the time series of power density and capacity factor estimated by both schemes are depicted in Fig. 8 for the three regions of interest (as shown in Fig. 5). These display the year-to-year changes in the seasonal cycle not evident in the averaged values from Fig. 7. All estimates indicate maximum values of power and capacity factor in winter (December–January) and minimum values in summer (June–August). For the neutral-based estimates, all three regions display similar patterns throughout the years. Region 2 is predicted to have the highest power potential, and region 1 is predicted to have the lowest. The differences between neutral-based power density estimates from region to region are large. For example, in January 2010, region 1 has power density of approximately $1050\,W\,m^{-2}$, region 2 has $1400\,W\,m^{-2}$, and region 3 has $900\,W\,m^{-2}$. For the same month, the differences are less extreme in the estimation of the capacity factor: 59%, 66%, and 54% for regions 1, 2, and 3, respectively. For all 5 years shown, the maximum capacity factor estimated for region 2 based on the neutral scheme is around 70% and the minimum is around 20%. For regions 1 and 3, the maximum is shifted a bit lower and is typically around 60%.

The stability-based estimates of power density and capacity factor differ from the neutral-based ones in that they predict the three regions to be more similar, though region 1 now exhibits the largest average power and capacity factor. This is not surprising given the typical stable conditions and 80-m wind estimates there (Figs. 4b,d). Particularly in the case of power density

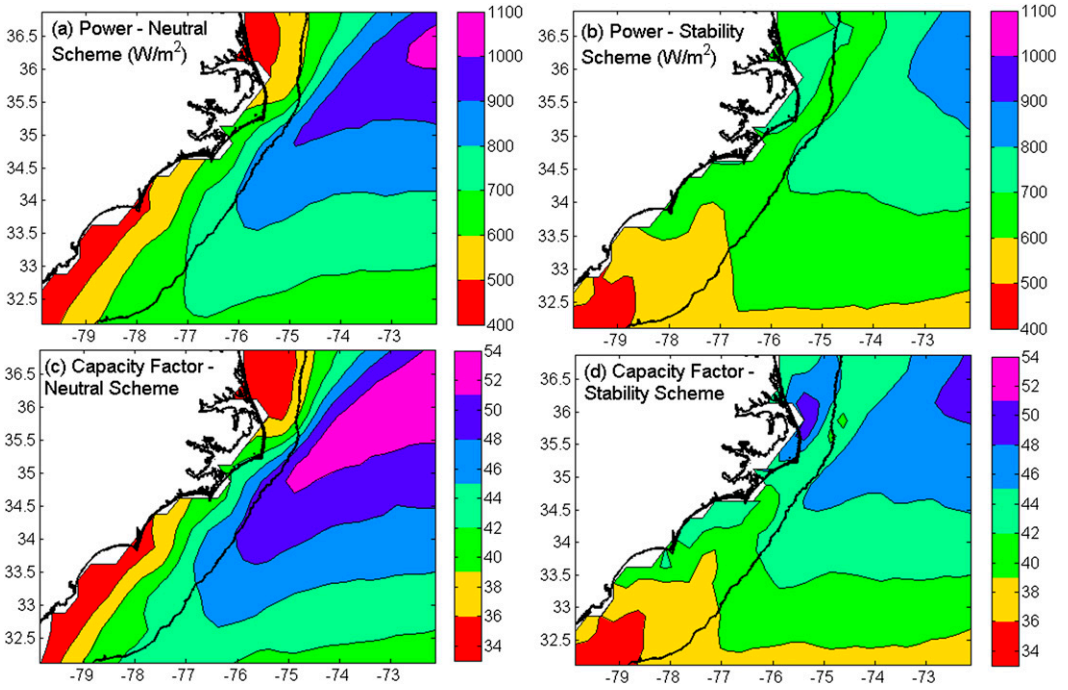

FIG. 7. Averages over the 2008–12 time period of power density (W m^{-2}) as estimated by the (a) neutral scheme and (b) stability scheme and capacity factor (%) as estimated by the (c) neutral scheme and (d) stability scheme.

(Fig. 8b), the estimate at region 1 is sometimes significantly higher than at the other two regions. For example, in March 2010, region 1 has power density of around 1450 W m^{-2}, region 2 has 1200 W m^{-2}, and region 3 has 1100 W m^{-2}. The capacity factor for region 1 for this month is 77%.

The interannual variability is also apparent. In Fig. 8a, region 2 has an annual maximum value of 1350 W m^{-2} in

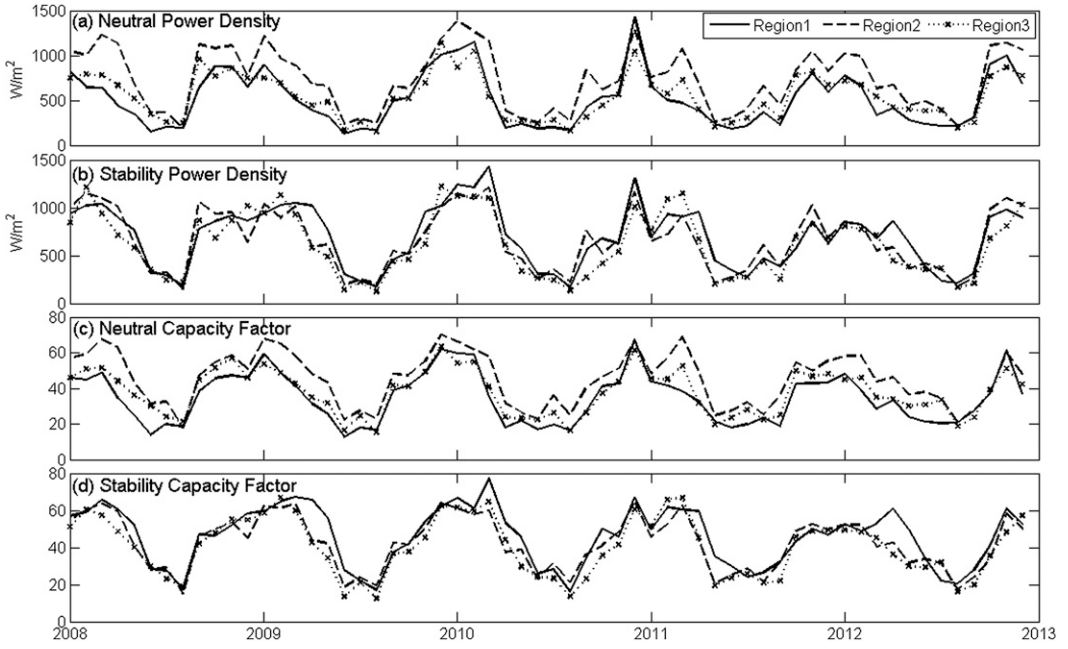

FIG. 8. Regional time series of power density as estimated by the (a) neutral scheme and (b) stability scheme and capacity factor as estimated by the (c) neutral scheme and (d) stability scheme. The averaging regions are as in Fig. 5.

January 2010 and an annual maximum of 990 W m^{-2} in January 2012. Similarly, in Fig. 8b, region 1 has a 2010 maximum of around 1450 W m^{-2} in March and a 2011 maximum of 850 W m^{-2} in April.

5. Discussion

There are several sources of uncertainty that arise from the data sources used in this study. The 10-m DASCAT winds were found to be more consistent with stability-based 10-m winds from the coastal buoys, rather than 10-m neutral winds. The geophysical model function used to estimate wind speed and direction from the scatterometer's backscatter measurements is based on comparison with collocated winds, converted to neutral 10-m wind, measured with globally distributed buoys and/or numerical weather prediction output (Hersbach 2010). A study of the relationship between the scatterometer's backscatter measurements and neutral and nonneutral winds finds no statistical difference (Portabella and Stoffelen 2009). The typically small differences between neutral and nonneutral winds, and uncertainty in the surface-layer models used to translate between the two representations of the wind field, are offered as explanations. These authors note that extreme stability and high wind speed conditions are poorly represented in the collocation datasets used and that further study of these conditions are warranted. Our finding of a better correlation of DASCAT winds with stability-based buoy winds is surprising but robust. We note that the bias in the neutral winds may result from factors other than atmospheric stability, for example, developing seas near the coastline. We intend to explore this topic further in an independent study.

A second and possibly dominant source of uncertainty is the impact of ocean currents on the wind speed estimates. As has been recently confirmed by observations (Plagge et al. 2012), scatterometers produce a wind estimate $\mathbf{U}_s$ relative to the ocean surface; referencing winds to Earth's surface $\mathbf{U}_e$ requires correction for ocean currents ($\mathbf{U}_o$), that is, $\mathbf{U}_e = \mathbf{U}_s + \mathbf{U}_o$, where $\mathbf{U}$ is a vector. The Gulf Stream is the dominant current in the study area. A recent study by Gula et al. (2015) finds mean surface currents in the study area up to 1.2 m s^{-1} in a jetlike structure of approximately 100-km width. The jet translates laterally on a variety of time scales, from days to months, over distances that can be greater than the width of the jet. Mean currents on the continental shelf are an order of magnitude smaller (Lentz 2008; Savidge and Bane 2001), though short-term currents can be considerably larger. There is not a standard ocean surface current product that can be used to reference the winds to Earth coordinates, and given that the correction is direction dependent, it is not obvious what impact it will have on the mean speeds formed in this study. As a simple exploration of the impact of a steady mean current on the average wind speed we compared the wind speed averaged over 1 yr from the satellite wind $\mathbf{U}_s$ with the wind speed averaged over 1 yr where a 1 m s^{-1} current to the northeast, intended to represent the Gulf Stream, was added to the satellite wind, effectively forming $\mathbf{U}_e$. A position over the Gulf Stream was chosen (34.375°N, 76.125°W). The vector average of $\mathbf{U}_s$ = (1.8, −0.9) m s^{-1}; adding $\mathbf{U}_o$ = (0.7, 0.7) m s^{-1} gives $\mathbf{U}_e$ = (2.5, −0.2) m s^{-1}. Wind speeds associated with the vector averages are quite different, $|\mathbf{U}_s| = 2.0$ m s^{-1} and $|\mathbf{U}_e| = 2.5$ m s^{-1}. Annually averaged wind speeds are much more comparable, 6.6 and 6.8 m s^{-1} for U_s and U_e, where the nonbold variables are magnitudes of the respective vectors, presumably because the variation in wind direction is nearly random with respect to the ocean current. The 0.2 m s^{-1} difference in wind speed is a 3% bias and can be considered a rough estimate of the magnitude of uncertainty due to the inability to correct the $\mathbf{U}_s$ for $\mathbf{U}_o$.

From the results presented in the previous section is it clear that the average low-level wind speed pattern (10 m) off North Carolina is highly structured. There are several physical features that drive the horizontal variability: the transition of the surface from land to water (the coastline); the presence of the Gulf Stream and the unstable atmospheric conditions it forces; and the wedge of cooler water off the northern Outer Banks, which promotes stable atmospheric conditions. How these features are manifest in the low-level and hub-height wind speeds is discussed next.

Low-level (10 m) wind speeds clearly increase moving offshore from the coastline (Fig. 4a), a reflection of decreased surface roughness (Garratt 1990). It is also clear that the sounds inshore from the Outer Banks support an increase in low-level winds off the shore of the Outer Banks, leading to the strongest winds along the coastline in the central portion of the state. Shore-parallel isotachs of wind speed in all of this study's depictions reflect the influence of this transition in surface roughness. The rapid increase in hub-height wind speed moving offshore is also obvious in other studies (e.g., Musial and Ram 2010; Gunturu and Schlosser 2012).

Farther offshore the persistent warm waters of the Gulf Stream present another change in surface conditions and almost always will drive convection in the overlying atmosphere. Momentum transfer at the surface is maximized by convection and has been observed to result in a covariation of SST and surface wind speed

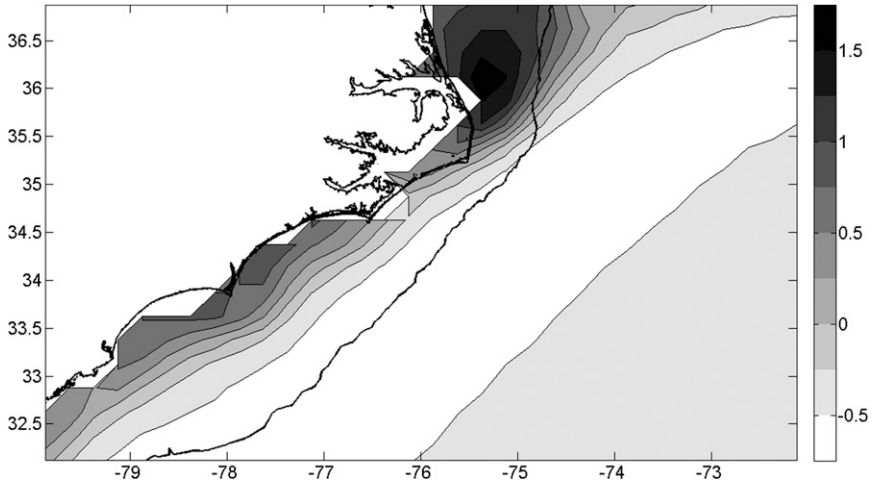

FIG. 9. Mean difference ($m\,s^{-1}$) between the 80-m wind estimates from the two height-adjustment schemes (stability − neutral) for the entire time range of 2008–12.

(O'Neill et al. 2012). The increased wind speeds in Fig. 4a over the region of greatest SST − SAT in Fig. 4b are consistent with this concept. Interestingly, the higher speeds over the Gulf Stream largely disappear in the winds adjusted to hub height using the stability-based scheme, suggesting that the influence of the surface conditions is on average a low-level phenomenon. It is physically sensible that the surface influence vanishes at some height above the surface but somewhat surprising that it might do so by 80 m. Our interpretation of the observed interannual variability (Fig. 6) presumes changing surface conditions lead to interannual variations. Variations in the depth of the surface boundary layer are to be expected and may explain this apparent discrepancy.

Last, the cooler SSTs on the continental shelf north of Cape Hatteras are capable of producing stable atmospheric conditions during nearly all times of year (e.g., Fig. 2). Strongly stable conditions over the ocean are uncommon (Garratt 1992) and in this case are maintained by advective processes in both the atmosphere and ocean. In the area off northeast North Carolina the stable conditions produce reduced surface winds but lead to a large increase in winds adjusted to hub height. Figure 9 displays the difference in average wind speed between the two techniques used in this study. The Gulf Stream's influence is obvious as the region of greatest reduction in wind speed using the stability-based scheme. The nearshore region and area off northeast North Carolina are influenced by periods of stable conditions and this leads to a greater estimate of the wind speed using the stability-based scheme. The differences, of 0.5–1.0 $m\,s^{-1}$ along the coastline and up to 2 $m\,s^{-1}$ off the shore of northeast North Carolina, indicate the importance of atmospheric stability on the structure of the surface boundary layer and wind resource assessment.

A recent study of wind shear and turbulence measured from a 95-m-tall tower in the North Sea 85 km from shore finds MOS theory to capture well unstable, neutral, and moderately unstable conditions ($z/L < 0.2$; Holtslag et al. 2015) at elevations up to the tower height. However, the slow growth and intermittent turbulence of strongly stable internal boundary layers (Mahrt 2014) over the sea calls into question the validity of the MOS scaling as it has been applied to each offshore location. The MOS scaling estimates the vertically unbounded steady-state profile and does not account for the time- (or space) dependent evolution of the boundary layer. The scheme cannot represent an internal boundary layer, where different surface conditions lead to the development of a new equilibrium structure. Since the MOS scheme cannot represent winds above the height of the internal boundary layer, at a point close to the transition from nonstable to stable surface forcing it will be likely to overestimate wind speed above the IBL. Thus along the horizontal boundaries of the regions of stable surface forcing there is a potential for a bias toward higher wind speeds using the stability-based extrapolation scheme.

It should be noted that the similarity solution of Garratt (1990) has been found to underestimate boundary layer thickness near the coast (within 20 km) in several offshore flow case studies (Mahrt et al. 2014; Vickers et al. 2001; Angevine et al. 2006) but to perform reasonably well farther offshore (Angevine et al. 2006). The boundary layer in these studies was found to grow to at least 50-m height over the first 10 km away from the coastline and reach to 100 m at greater distances.

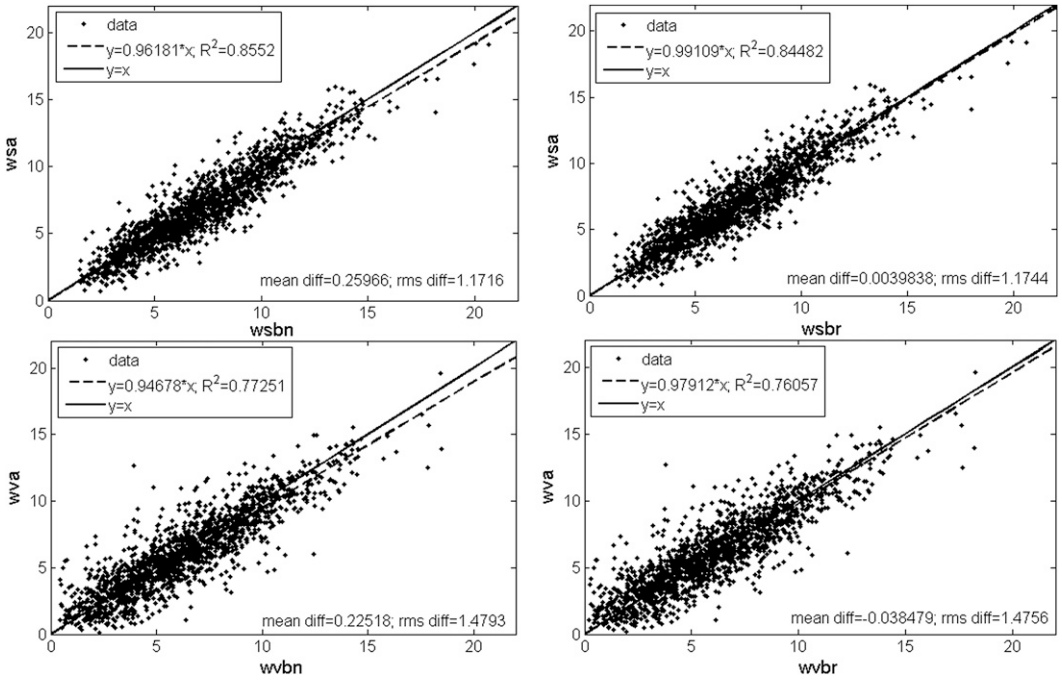

FIG. A1. Comparison between DASCAT and buoy winds ($m\,s^{-1}$) at station 41013. Comparisons include wsa and wva with wsbr, wsbn, wvbr, and wvbn. Mean differences correspond to buoy winds − DASCAT winds.

The present study improves on an earlier regional assessment (UNC 2009; Seim et al. 2010) of the wind field off the shore of North Carolina by using data sources that extend farther offshore and by utilizing more sophisticated boundary layer formulations. Capacity factors (formed using a Vestas V90 power curve) over coastal waters estimated assuming neutral stability (Fig. 7c) are comparable to those estimated using a spatially varying power-law height-adjustment (for details see UNC 2009; Seim et al. 2010). The present study finds somewhat higher values off the central coast, but the position of the 35% contour off the northern and southern coasts is quite similar. The high values farther offshore confirm the general pattern of increased capacity factor over the Gulf Stream and farther offshore. Capacity factors estimated using the stability-based extrapolation scheme exhibit a different spatial pattern, being less variable cross-shore and exhibiting more along shelf changes, with values around 40% for most of the coastal area south of Cape Hatteras but greater than 45% north of Cape Hatteras. A pattern of increased capacity factor to the north is seen, mimicking the speed and power density distributions.

6. Summary

The aim of this study was to incorporate stability conditions into a turbine-height estimate of the regional wind resource off the shore of North Carolina. This was performed using the 10-m DASCAT wind field and the inclusion of other data. It was established that the North American Regional Reanalysis product overestimates several of the data variables needed for a stability-based extrapolation scheme in this region. Specifically, the SST is overestimated by 1.2°–3.0°C, SAT by 0.9°–1.9°C, and dewpoint by 2.2°–3.7°C. Furthermore, the NARR data overestimate the sea–air temperature difference (SST − SAT), resulting in persistent unstable conditions, when in reality stable conditions are present in certain regions and seasons in the study area. The substitution of AVHRR-OI SST helps to minimize this issue, and in fact shifts the bias in the other direction (somewhat overestimating the occurrence of stable conditions).

The DASCAT-measured wind field, found to correlate best with the actual 10-m buoy observations over coastal waters, reveals that the 10-m winds off the shore of North Carolina are in the range of 6.5–9.0 $m\,s^{-1}$ on average. If neutral stability is assumed, the winds at a turbine height of 80 m are estimated to be 7.5–10.5 $m\,s^{-1}$. If, instead, atmospheric stability is taken into account, the structure of the wind field is much different at 80 m and is predicted to be up to 10 $m\,s^{-1}$ on average in some regions. The predictions from the two methods differ most notably in the coastal region north of Cape Hatteras, where stable conditions are prevalent and the

TABLE A1. Statistics of comparison between wsa and wva and wsbr, wsbn, wvbr, and wvbn. The linear regression coefficient, R^2 of the fit, mean difference, and rms difference for various pairings are shown. In all cases DASCAT winds were subtracted from buoy winds to form differences.

	wsa				wva			
	Regression coef	R^2	Mean diff ($m\,s^{-1}$)	rms diff ($m\,s^{-1}$)	Regression coef	R^2	Mean diff ($m\,s^{-1}$)	rms diff ($m\,s^{-1}$)
wsbr								
41001	1.003	0.68	−0.18	1.88	0.873	0.57	0.9	2.45
41004	0.981	0.83	0.08	1.18	0.86	0.74	1.01	1.81
41013	0.989	0.85	0.02	1.17	0.866	0.73	0.96	1.87
41025	0.998	0.8	−0.08	1.41	0.877	0.68	0.94	2.11
41036	0.999	0.81	−0.08	1.32	0.873	0.71	0.92	1.94
44014	0.996	0.81	−0.01	1.39	0.856	0.69	1.06	2.1
wsbn								
41001	0.977	0.69	0.08	1.85	0.849	0.57	1.17	2.54
41004	0.952	0.84	0.33	1.18	0.832	0.74	1.26	1.95
41013	0.962	0.86	0.26	1.17	0.84	0.73	1.22	2
41025	0.973	0.79	0.14	1.44	0.853	0.66	1.18	2.26
41036	0.972	0.82	0.16	1.31	0.847	0.71	1.18	2.06
44014	0.992	0.82	−0.01	1.36	0.85	0.7	1.08	2.11
wvbr								
41001					0.969	0.61	−0.06	2.12
41004					0.967	0.75	0.05	1.46
41013					0.979	0.76	−0.04	1.48
41025					0.987	0.73	−0.1	1.69
41036					0.979	0.69	−0.13	1.71
44014					0.965	0.73	0.06	1.69
wvbn								
41001					0.942	0.63	0.22	2.01
41004					0.934	0.77	0.32	1.46
41013					0.947	0.77	0.23	1.48
41025					0.958	0.73	0.14	1.72
41036					0.948	0.71	0.13	1.69
44014					0.958	0.73	0.07	1.7

sea–air temperature difference is negative in the average. In this region, the 80-m wind speed difference (stability-based estimate minus neutral estimate) is up to $2\,m\,s^{-1}$ in the average.

Power densities assuming neutral atmospheric conditions are 400–800 $W\,m^{-2}$ on average in water depths less than 100 m. The stability-based estimate predicts a similar range of power density values but of differing spatial structure, with a maximum in the region north of Cape Hatteras. Because of this region, where cool waters frequently lead to stable conditions, and the Gulf Stream, which leads to unstable conditions, North Carolina is a particularly interesting region to conduct a stability-based study of the wind resource.

Seasonal variations lead to maximum winds in winter for most of the area under study. Stable conditions in late winter and spring produce annual maximum winds off northeast North Carolina and along the nearshore region, the strength of which is modulated interannually. A brief but distinct annual minimum is observed in August, when speeds on average drop below $7.5\,m\,s^{-1}$ at hub height.

The stability-based estimate of hub-height winds differs significantly from the neutral-based estimate. Further study of the appropriateness of the scheme during stable conditions and validation of the estimated wind patterns are needed to better constrain the wind resource in this dynamic coastal setting. Observations of wind profiles and appropriate ancillary data in locations with contrasting stability are needed to validate that the MOS scaling is applicable. Internal boundary layer height observations over the region would clarify the vertical extent of the surface boundary layer and whether turbines would reside wholly within the boundary layer or span the transition above it. This type of information would be important to engineers and operators because it would define the vertical shear experienced by the turbines. Significant shear could produce differential loading at the top and bottom of the swept area and have implications for design and maintenance of the turbines.

Acknowledgments. Support from Duke Energy for the authors is gratefully acknowledged. Ashley Mui, Jenna

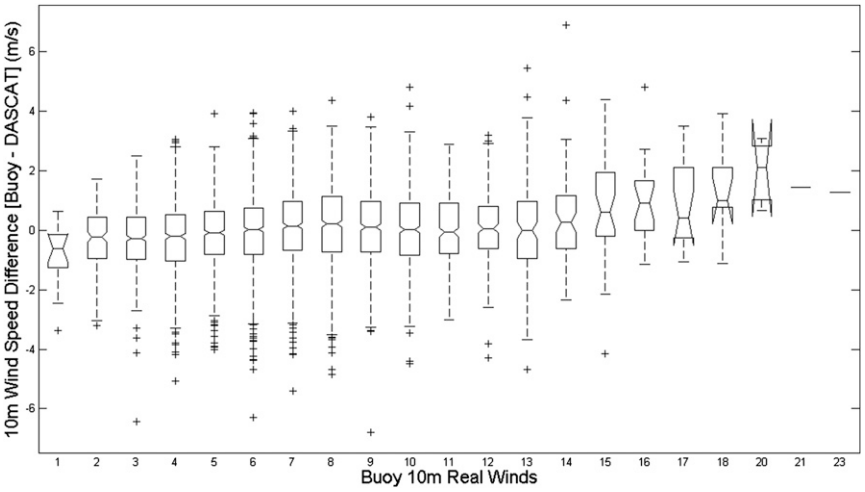

FIG. A2. Box plot of the difference in 10-m speed (buoy actual 10-m wind speed − DASCAT) as a function of buoy wind speed. The horizontal line marks the median, the box marks the interquartile range (IQR), the dashed lines mark the range of values up to 1.5 times the IQR, and plus signs are outliers. The notch in the box marks 95% confidence bounds on the median and reflects the number of values in each speed range. Few data points exist below 1.5 m s^{-1} or above 14.5 m s^{-1}; the odd shape of the IQR at high velocities results from the notch being greater than the IQR.

Koester, and Rick Browne contributed to initial analyses. We also acknowledge three anonymous reviewers whose comments significantly improved the manuscript.

APPENDIX

Validation of Satellite Winds

ASCAT winds are derived using empirical geophysical model functions that relate the measured microwave backscatter signal to the 10-m neutral wind. The C-band model 5.N (CMOD5.N; Hersbach 2010) is essentially the model developed for nonneutral 10-m winds, CMOD5, with a 0.5 m s^{-1} bias correction (relative to buoy observations) and a 0.2 m s^{-1} offset to account for the average difference between neutral and nonneutral winds. Validity of level-2 (L2) 12.5-km-resolution ASCAT estimates near a coastline, which are the source of information used in the L3 daily product used in this study, have been found to be valid within 15–20 km of the coastline (Verhoef et al. 2012). The two DASCAT wind products, the daily wind speed and daily wind vector, are evaluated against buoy observations.

Buoy winds were measured hourly at six locations shown in Fig. 1. Buoy 41001 is located in deep water in the Sargasso Sea, while the rest are coastal buoys moored in depths of 70 m or less. Hourly winds were adjusted to 10-m height using COARE v3.0 to produce stability-dependent and neutral winds (Fairall et al. 2003). Two forms of daily average wind speeds were created for both actual and neutral winds, one that averages the hourly wind speed (wsbr and wsbn), the other that averages the hourly wind components (zonal and meridional) to form a daily wind vector, the magnitude of which is a second wind speed (wvbr and wvbn). These daily values were then paired with the DASCAT wind speed (wsa) and the wind speed formed as the magnitude of the DASCAT wind components (wva).

Scatterplots of the various combinations, fits to $y = ax$, and mean differences, and the rms difference were formed. Figure A1 is an example for buoy 41013. The figure makes clear that wind speed averages exhibit the highest correlation. The vector-averaged daily wind speed is significantly lower on average than the daily averaged wind speed and exhibits the lowest correlation.

Table A1 summarizes the comparison of buoy and DASCAT wind speeds, using the regression coefficient a, R^2 of the regression, the mean difference, and rms difference. It includes actual (wsbr) and neutral (wsbn) buoy winds. For all coastal buoys (i.e., other than 41001) the best correlation is between wsa and wsbr. Regression coefficients are 0.98–1, R^2 values are 0.8 or higher, the absolute value of the mean differences are less than 0.1 m s^{-1}, and rms difference values are 1.4 m s^{-1} or less. Wsa and wsbn are also well correlated but regression coefficients are slightly lower and mean differences are as high as 0.33 m s^{-1}, indicating a worse fit than to the actual buoy wind speed. The exception is the deep-water buoy,

41001, which has lower R^2 values and higher rms differences in all the comparisons but for which the neutral buoy wind speed exhibits a lower mean difference than for the actual buoy wind speed. DASCAT vector-averaged wind speed (wva) is noticeably smaller than wsbr and wsbn, with regression coefficients of 0.83–0.88 and mean differences of $1\,m\,s^{-1}$ or greater. Actual vector-averaged buoy wind speed (wvbr) correlates well with wva, exhibiting regression coefficients of 0.96–0.99 but somewhat larger mean differences and rms differences and lower R^2 values than for the wind speed comparison. Thus the DASCAT wind speed is best interpreted as the actual 10-m wind speed for the coastal region under study. The one buoy in deeper water suggests that moving offshore the DASCAT wind speed may be more representative of the 10-m neutral wind speed. Given that utility-scale wind farms to date are all on shallow continental shelves, we choose to treat the DASCAT winds as actual 10-m winds for this study, acknowledging increasing uncertainty in the estimates moving farther from shore.

There is only a slight bias among the coastal buoys for lower wind speeds (Fig. A2; DASCAT winds greater than buoy winds for speeds $< 2\,m\,s^{-1}$) and a more noticeable bias at higher wind speeds (daily ASCAT winds less than buoy winds for speeds $> 14\,m\,s^{-1}$). However, neither speed range is well populated and uncertainties are large. There is no distinction between the speed-dependent difference when using nonneutral versus neutral buoy winds (not shown), and therefore the difference in bias is not a result of poor performance over a limited range of wind speed.

REFERENCES

Angevine, W. M., J. E. Hare, C. W. Fairall, D. E. Wolfe, R. J. Hill, W. A. Brewer, and A. B. White, 2006: Structure and formation of the highly stable marine boundary layer over the Gulf of Maine. *J. Geophys. Res.*, **111**, D23S22, doi:10.1029/2006JD007465.

Bentamy, A., and D. Croize-Fillon, 2012: Gridded surface wind fields from Metop/ASCAT measurements. *Int. J. Remote Sens.*, **33**, 1729–1754, doi:10.1080/01431161.2011.600348.

CERSAT, 2012: Seawinds on ASCAT level 3 gridded mean wind fields in 0.25° geographical grid. IFREMER/Centre ERS d'Archivage et de Traitement. Subset used: 2008–14, accessed April 2013 and March 2015. [Available online at http://products.cersat.fr/details/?id=CER_WND_GLO_1D_025_MWF_ASCAT.]

Edson, J., and Coauthors, 2013: On the exchange of momentum over the open ocean. *J. Phys. Oceanogr.*, **43**, 1589–1610, doi:10.1175/JPO-D-12-0173.1.

Fairall, C. W., E. F. Bradley, D. P. Rogers, J. B. Edson, and G. S. Young, 1996: Bulk parameterization of air-sea fluxes for Tropical Ocean-Global Atmosphere Coupled-Ocean Atmosphere Response Experiment. *J. Geophys. Res.*, **101**, 3747–3764, doi:10.1029/95JC03205.

——, ——, J. Hare, A. Grachev, and J. Edson, 2003: Bulk parameterization of air-sea fluxes, update and verification for the COARE algorithm. *J. Climate*, **16**, 571–591, doi:10.1175/1520-0442(2003)016<0571:BPOASF>2.0.CO;2.

Furevik, B. R., A. M. Sempreviva, L. Cavaleri, J. M. Lafevre, and C. Transerici, 2011: Eight years of wind measurements from scatterometer for wind resource mapping in the Mediterranean Sea. *Wind Energy*, **14**, 355–372, doi:10.1002/we.425.

Garratt, J. R., 1990: The internal boundary layer—A review. *Bound.-Layer Meteor.*, **50**, 171–203, doi:10.1007/BF00120524.

——, 1992: *The Atmospheric Boundary Layer*. Cambridge University Press, 316 pp.

Godfrey, J. S., and A. C. M. Beljaars, 1991: On the turbulent fluxes of buoyancy, heat and moisture at the air-sea interface at low wind speeds. *J. Geophys. Res.*, **96**, 22 043–22 048, doi:10.1029/91JC02015.

Gula, J., M. J. Molemaker, and J. C. McWilliams, 2015: Gulf Stream dynamics along the southeastern U.S. seaboard. *J. Phys. Oceanogr.*, **45**, 690–715, doi:10.1175/JPO-D-14-0154.1.

Gunturu, U. B., and C. A. Schlosser, 2012: Characterization of wind power resources in the United States. *Atmos. Chem. Phys.*, **12**, 9687–9702, doi:10.5194/acp-12-9687-2012.

Hersbach, H., 2010: Comparison of C-band scatterometer CMOD5.N equivalent neutral winds with ECMWF. *J. Atmos. Oceanic Technol.*, **27**, 721–736, doi:10.1175/2009JTECHO698.1.

Holtslag, M. C., W. A. A. M. Bierbooms, and G. J. V. van Bussel, 2015: Validation of surface layer similarity theory to describe far offshore marine conditions in the Dutch North Sea in scope of wind energy research. *J. Wind Eng. Ind. Aerodyn.*, **136**, 180–191, doi:10.1016/j.jweia.2014.10.013.

Karagali, I., A. Peña, M. Badger, and C. B. Hasager, 2014: Wind characteristics in the North and Baltic Seas from the QuikSCAT satellite. *Wind Energy*, **17**, 123–140, doi:10.1002/we.1565.

Karamanis, D., C. Tsabaris, K. Stamoulis, and D. Georgopoulos, 2011: Wind energy resources in the Ionian Sea. *Renewable Energy*, **36**, 815–822, doi:10.1016/j.renene.2010.08.007.

Lee, M. E., G. Kim, S.-T. Jeong, D. H. Ko, and K. S. Kang, 2013: Assessment of offshore wind energy at Younggwang in Korea. *Renewable Sustain. Energy Rev.*, **21**, 131–141, doi:10.1016/j.rser.2012.12.059.

Lentz, S., 2008: Observations and model of the mean circulation over the middle Atlantic Bight continental shelf. *J. Phys. Oceanogr.*, **38**, 1203–1221, doi:10.1175/2007JPO3768.1.

Mahrt, L., 2014: Stably stratified atmospheric boundary layers. *Annu. Rev. Fluid Mech.*, **46**, 23–45, doi:10.1146/annurev-fluid-010313-141354.

——, D. Vickers, and E. L Andreas, 2014: Low-level wind maxima and structure of the stably stratified boundary layer in the coastal zone. *J. Appl. Meteor. Climatol.*, **53**, 363–376, doi:10.1175/JAMC-D-13-0170.1.

Mesinger, F., and Coauthors, 2006: North American Regional Reanalysis. *Bull. Amer. Meteor. Soc.*, **87**, 343–360, doi:10.1175/BAMS-87-3-343.

Musial, W., and B. Ram, 2010: Large-scale offshore wind power in the United Sates: Assessment of opportunities and barriers. NREL Tech. Rep. NREL/TP-500-40745, 240 pp., doi:10.2172/990101.

NCDC, 2007: GHRSST level 4 AVHRR_OI global blended sea surface temperature analysis; NASA PO.DAAC. NOAA/National Climatic Data Center. Subset used: 2008–12, accessed October 2012 and September 2013, doi:10.5067/GHAAO-4BC01.

O'Neill, L., D. Chelton, and S. Esbensen, 2012: Covariability of surface wind and stress responses to sea surface temperature fronts. *J. Climate*, **25**, 5916–5942, doi:10.1175/JCLI-D-11-00230.1.

Pimenta, F., W. Kempton, and R. Garvine, 2008: Combining meteorological stations and satellite data to evaluate the offshore wind power resource of southeastern Brazil. *Renewable Energy*, **33**, 2375–2387, doi:10.1016/j.renene.2008.01.012.

Plagge, A., D. Vandemark, and B. Chapron, 2012: Examining the impact of surface currents on satellite scatterometer and altimeter ocean winds. *J. Atmos. Oceanic Technol.*, **29**, 1776–1793, doi:10.1175/JTECH-D-12-00017.1.

Portabella, M., and A. Stoffelen, 2009: On scatterometer ocean stress. *J. Atmos. Oceanic Technol.*, **26**, 368–382, doi:10.1175/2008JTECHO578.1.

PSD, 2006. National Centers for Environmental Prediction (NCEP) reanalysis products. NOAA/OAR/ESRL/Physical Sciences Division. Subset used: 2008–12, monolevels (prmsl, air.sfc, air.2m, rhum.2m, uwnd.10m, vwind.10m), accessed February 2012, August 2012, and March 2013. [Available online at http://www.esrl.noaa.gov/psd/data/gridded/data.narr.html.]

Reynolds, R. W., T. M. Smith, C. Liu, D. B. Chelton, K. S. Casey, and M. G. Schlax, 2007: Daily high-resolution-blended analyses for sea surface temperature. *J. Climate*, **20**, 5473–5496, doi:10.1175/2007JCLI1824.1.

Savidge, D., and J. Bane, 2001: Wind and Gulf Stream influences on along-shelf transport and off-shelf export at Cape Hatteras, North Carolina. *J. Geophys. Res.*, **106**, 11 505–11 527, doi:10.1029/2000JC000574.

Seim, H., S. Haines, B. Edwards, and J. Cleary, 2010: An initial evaluation of offshore wind energy potential off the coast of North Carolina. *Fifth Int. Symp. on Computational Wind Engineering (CWE2010)*, Chapel Hill, NC, IAWE, paper 504. [Available online at ftp://ftp.atdd.noaa.gov/pub/cwe2010/Files/Papers/504_seim.pdf.]

——, A. Mui, N. Thomas, and S. Haines, 2012: Impact of atmospheric stability on wind resource estimates off North Carolina. *Proc. Oceans, 2012*, Hampton Roads, VA, IEEE, doi:10.1109/OCEANS.2012.6404944.

Sheridan, B., S. D. Baker, N. S. Pearre, J. Firestone, and W. Kempton, 2012: Calculating the offshore wind power resource: Robust assessment methods applied to the U.S. Atlantic coast. *Renewable Energy*, **43**, 224–233, doi:10.1016/j.renene.2011.11.029.

UNC, 2009: Coastal wind: Energy for North Carolina's future: A study of the feasibility of wind turbines in the Pamlico and Albemarle Sounds and in ocean waters off the North Carolina coast. University of North Carolina at Chapel Hill Rep., 378 pp. [Available online at https://www.climate.unc.edu/Portals/Climate/Coastal%20Wind-%20Energy%20for%20NC2019s%20Future.pdf.]

Verhoef, A., M. Portabella, and A. Stoffelen, 2012: High-resolution ASCAT scatterometer winds near the coast. *IEEE Trans. Geosci. Remote Sens.*, **50**, 2481–2487, doi:10.1109/TGRS.2011.2175001.

Vickers, D., L. Mahrt, J. Sun, and T. Crawford, 2001: Structure of offshore flow. *Mon. Wea. Rev.*, **129**, 1251–1258, doi:10.1175/1520-0493(2001)129<1251:SOOF>2.0.CO;2.

Zheng, C., J. Pan, and J. Li, 2013: Assessing the China Sea wind energy and wave energy resources from 1988 to 2009. *Ocean Eng.*, **65**, 39–48, doi:10.1016/j.oceaneng.2013.03.006.